Breakdown of the quantum Hall effect as a function of the filling factor and the contact configuration

1992 J. Phys.: Condens. Matter 4 4003

(http://iopscience.iop.org/0953-8984/4/15/014)

J. Phys.: Condens. Matter 4 (1992) 4003–4015. Printed in the UK

Breakdown of the quantum Hall effect as a function of the filling factor and the contact configuration

G Nachtwei, C Breitlow, A Jaeger and J Breitlow-Hertzfeldt
Humboldt-Universität zu Berlin, Institut für Festkörperphysik, Invalidenstrasse 110, D-O1040 Berlin, Federal Republic of Germany

Received 6 August 1991, in final form 30 December 1991

Abstract. The filling-factor dependence of the critical current of the quantum Hall effect (QHE) was measured using several current and voltage contact configurations on Si metal–oxide–semiconductor and Si metal–nitride–oxide–semiconductor Hall bars and Corbino rings. The results indicate that the breakdown is dominated by different mechanisms in different current and filling-factor regimes. The critical current is primarily dependent on the position of the current-injecting contact with respect to the Hall field polarity. At higher currents the data cannot be explained by an edge channel picture. Estimates on the basis of several breakdown mechanisms and calculations based upon a Zener tunnelling model were made to explain the experimental results. The Zener tunnelling model provides the best quantitative results if a filling-factor-dependent width of the quantum Hall current path is introduced. The current path width is maximal near integer filling factors and decreases with deviation from the plateau centre. Our results confirm that the breakdown of the QHE is a local phenomenon.

1. Introduction

A whole variety of experimental and theoretical work has been done since the early 1980s to clarify the current flow mechanism in the quantum Hall (QH) regime and its breakdown. Despite all these efforts the problem is still not fully understood [1–3]. Furthermore, some of the experimental data and their interpretation are in contradiction with one another so that the assumption of different mechanisms dominating the various measuring geometries [3, 4], materials [5] and current levels [6–8] appears to be reasonable. Measurements of the electrostatic potential distribution on GaAs/GaAlAs heterojunctions under QH conditions by the application of the Pockels effect [9, 10] yielded a potential drop of about 80% of the entire Hall voltage near the sample boundaries. However, the width and the direction of the current paths deduced from the measurements are not easily reconcilable with the widely used edge current picture [11] at the current level used in these experiments.

Breakdown measurements on macroscopic Hall bars [12–16] were interpreted using the hot-electron model [16], phonon-assisted electron transfer between the sample edges [17], the assumption of an increase of delocalized states with the Hall field, which reduces the distance of the mobility edge of the next Landau band to the Fermi energy [18], resonant tunnelling [19] and Zener tunnelling [20]. The preferred models to explain the breakdown experiments performed on samples with narrow constrictions [21, 22] or entirely mesoscopic dimensions [23] are the quasi-elastic inter-Landau-level scattering (QUILLS) [24] or the edge current model [25].

0953-8984/92/154003+13$04.50

Recent experiments of van Son *et al* propose a local breakdown starting from the current-injecting contact [3, 15]. Time-resolved measurements of the breakdown revealed dissipative states characterized by voltage differences of $\hbar\omega_c/e$ ($\hbar\omega_c$ = cyclotron energy, e = electron charge) [26].

We measured the breakdown characteristics of the quantum Hall effect (QHE) on Si metal–oxide–semiconductor and Si metal–nitride–oxide–semiconductor (MOS and MNOS) samples with ordinary macroscopic Hall bar geometry for several current-injecting and voltage-probing contact configurations. Furthermore, we compared the results to those obtained on Corbino rings located on the same chips.

We explain the filling-factor-dependent measurements by a Zener tunnelling model with a filling-factor-dependent width of the low dissipative current path. Whereas the tunnelling picture yields appropriate results at higher Hall fields, a different mechanism apparently dominates the breakdown of the QHE at lower critical currents.

From the data obtained we conclude that the position of the electron-injecting contact referring to the Hall field polarity is essential for the critical current level. Former assumptions of different current flow mechanisms at different current levels [6–8] are confirmed by the present results.

2. Sample characteristics

The Si metal–insulator–semiconductor (MIS) structures used for this study were produced with an insulator thickness of 400 nm SiO_2 (MOS) or 350 nm SiO_2/80 nm Si_3N_4 (MNOS). The maximum mobilities of the MOS and MNOS structures at $T = 1.3$ K are 1.34×10^4 and 2.37×10^4 cm^2 V^{-1} s^{-1}, respectively. The insulator capacity per area dn_s/dV_g varies from 4.73×10^{10} to 5.15×10^{10} cm^{-2} V^{-1}.

The sample geometry of the Hall bars is characterized by three equally spaced pairs of potential contacts (probe width 2 μm) 500 μm apart from one another and 1 mm from the current contacts and a channel width w of 300 μm. The Corbino 'rings' are regular octagons with an inner diameter of 200 μm and a 'channel width' of 100 μm. The sample geometries are sketched in figure 1. Further information concerning the samples can be obtained from [27, 28].

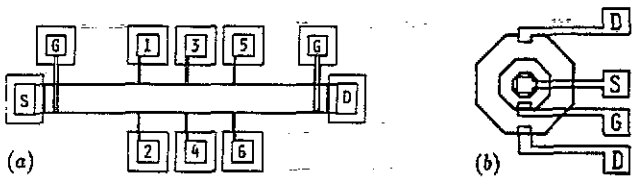

Figure 1. Sample geometry: (*a*) Hall bar; (*b*) Corbino ring. S, source; D, drain; G, gate; 1–6, potential probes.

Magnetic fields up to 12 T were generated using a superconducting solenoid. The sample temperature of $T = 1.3$ K was maintained by pumping the helium bath in a separate sample cryostat. This temperature is low enough to realize the QH regime in our samples for $B > 10$ T [28]. The measurements were done using DC currents supplied by a ground-free battery-operated source. The gate voltages were

also generated by batteries. To avoid a possible lattice heating of the samples at higher current levels (maximum power input 70 μW), the sample was placed in immediate thermal contact with a copper cylinder. This cylinder was cooled by liquid helium and contained a temperature sensor (carbon resistor) with a temperature resolution better than 0.1 K. The data were taken by a high-resolution digital data processing system including two $6\frac{1}{2}$ digit precision voltmeters. The sample currents were measured using a calibrated normal resistor. The resistance resolution of the measuring set-up was between 0.1 and 0.001 Ω for sample currents of 0.7 $\mu A < I_{SD} < 100$ μA.

3. Experimental results and conclusions

3.1. Breakdown at Hall bars

We have investigated the source-drain current dependence of the plateau width of the $i = 4$ plateau at MOS (H VI, H VII) and MNOS (H IX) samples with Hall bar geometry in the current range 0.7 $\mu A \leqslant I_{SD} \leqslant 100$ μA at a temperature of $T = 1.3$ K. The plateau width was determined by sweeping the gate voltage V_g at a fixed magnetic field value of $B = 11.56$ T. The plateau was defined in that range of the gate voltage with ρ_{xx} being below threshold values ρ_{xx}^{th} of various amounts from 0.01 Ω up to 10 Ω, instead of using the more arbitrary criterion of a threshold voltage V_s. A threshold value in ρ_{xx} corresponds to a critical Hall angle θ ($\tan\theta = \rho_{xy}/\rho_{xx}$, $\theta = \pi/2$ for ideal non-dissipative current transport) or to a critical share of power $\delta p/p = \cos\theta$ that is dissipated in the sample apart from the zones with steep potential gradients at the source and drain contacts.

Figure 2 shows a set of ρ_{xx} and ρ_{xy} traces as a function of the gate voltage for several values of I_{SD} measured on sample H VII. From both the ρ_{xx} and ρ_{xy} traces the reduction of the plateau width with increasing current is apparent. Applying the threshold condition mentioned above to the ρ_{xx} traces, we can deduce the dependence of the critical current of the $i = 4$ QH state on the gate voltage or the filling factor, respectively. Two main features are obvious for all threshold values ρ_{xx}^{th} shown in figure 3(*a*): the dependences are not triangular (see e.g. [23]) and they are asymmetric with respect to the plateau centre at $I_{SD} \to 0$. In the current region 0.7 $\mu A \leqslant I_{SD} \leqslant 7$ μA the plateau width is strongly decreasing. For currents 20 $\mu A \leqslant I_{SD} \leqslant 50$ μA it remains almost unchanged. (Slight increases as for the low-voltage side at $\rho_{xx}^{th} = 0.01$ Ω presented in figure 3 mean a switching from a lower dissipative to a higher dissipative and back to a lower dissipative current transport regime with increasing current level at a fixed gate voltage and will be discussed below.) At higher currents the plateau width decreases again and almost disappears at 100 μA. This general behaviour was found for all MOS structures investigated (see figure 3(*b*) of H VI) with similar mobility values and 'standard' geometry. The asymmetry observed is due to the reduction of the effective gate voltage with increasing source–drain current. The increasing Hall voltage (and simultaneously the source–drain voltage) causes an inhomogeneous carrier distribution with an average value determined by the effective gate voltage V_g^{eff}:

$$V_g^{eff} = V_g - h \times I_{SD}/2ie^2. \tag{1}$$

This effect yields a reduction of the effective gate voltage by 0.316 V for a current increase up to $I_{SD} = 98$ μA (sample H VII at $B = 11.56$ T). Hence, the gate

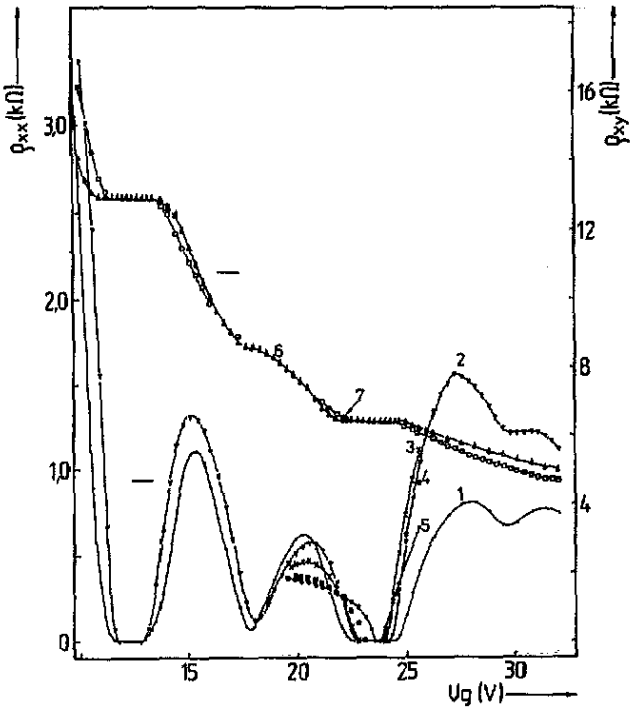

Figure 2. Resistivity ρ_{xx} (curves 1–5) and Hall resistivity ρ_{xy} (curves 6 and 7) versus gate voltage V_g at $B = 11.56$ T and $T = 1.3$ K for different source–drain currents (H VII, MOS): 1 and 6, $I_{SD} = 0.7$ μA; 2 and 7, $I_{SD} = 6.8$ μA; 3, $I_{SD} = 18.8$ μA; 4, $I_{SD} = 43.0$ μA; 5, $I_{SD} = 98.0$ μA.

voltage has to be increased by the corresponding amount (see figure 3) to reach the plateau centre ($\nu = i = 4$) at higher values of I_{SD}.

Figure 3(*c*) shows the critical current dependence on the filling factor for a MNOS sample (H IX). The plateau width at medium current levels is smaller compared to the MOS samples owing to the higher mobility and the lower density of states (DOS) of the MNOS samples [28]. Furthermore, the critical current at its maximum amounts to only 30 μA for $\rho_{xx}^{th} = 0.1$ Ω.

The plateau width shows a tail-like enhancement towards higher gate voltages for currents below 2 μA. Assuming a filling factor of 4.0 in the middle of the plateau at low currents, a current increase shifts the plateau centre towards lower gate voltages. This corresponds to a sudden increase of the filling factor and the carrier density for currents above 2.0 μA at a fixed gate voltage. Possible explanations could be given by a sudden reduction of the DOS in the low-energy tail of the lowest $l = 1$ quantum level or a sudden decrease of its mobility edge above a critical Hall field [18]. We attribute the effect to inhomogeneities of the carrier distribution along the sample (see below), leading to carrier redistributions at a certain level of the Hall field. The presence of stronger inhomogeneities reduces the area of the QH current flow (see below), and the lower maximal critical current would be a natural consequence. However, these inhomogeneities should be rather macroscopic (owing to long-range potential fluctuations) because of the higher Hall mobility compared to the MOS samples.

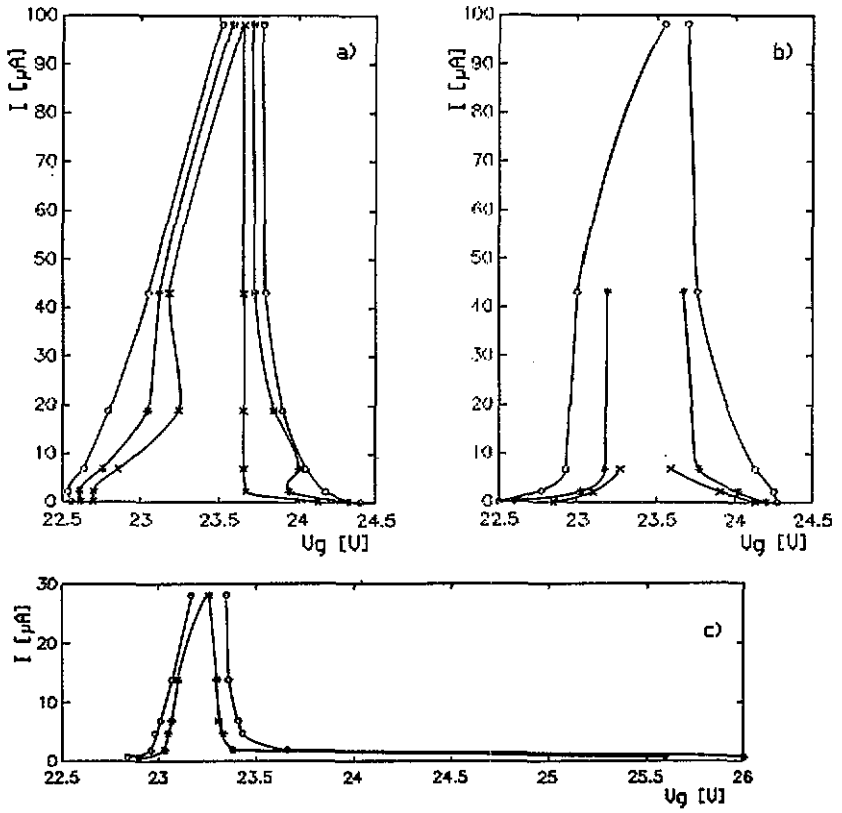

Figure 3. Gate voltage range of the $i = 4$ plateau ($B = 11.56$ T, $T = 1.3$ K) determined by (×) $\rho_{xx} < 0.01\ \Omega$, (*) $\rho_{xx} < 0.1\ \Omega$, (○) $\rho_{xx} < 1\ \Omega$, for (*a*) sample H VII (MOS), (*b*) sample H VI (MOS) and (*c*) sample H IX (MNOS).

Various models were proposed to explain the breakdown in macroscopic samples [12–16]. We have tested the applicability of some of the models to interpret our results. First, we calculated the drift velocity v_{DC} corresponding to the maximal critical current I_c of the $i = 4$ plateau:

$$v_{DC} = \epsilon_{HC}/B = hI_c/ie^2Bw \tag{2}$$

where ϵ_{HC} = critical Hall field. We obtained $v_{DC} = 186$ m s^{-1} for sample H VII (MOS) and $v_{DC} = 56$ m s^{-1} for sample H IX (MNOS). These values are smaller than the lowest sound velocity in silicon ($v_s = 3764$ m s^{-1} [29]) by more than one order of magnitude. However, equation (2) implies a homogeneous current flow over the entire channel width. To fulfil the condition for a QHE breakdown induced by spontaneous phonon emission ($v_{DC} \geqslant v_s$) [17], the current flow had to be restricted to about 1/20th or 1/60th of the channel width, respectively. This is possible in view of the strongly inhomogeneous Hall potential distribution obtained from experiments [30, 31] and theories [32, 33]. The filling-factor dependence of the critical current observed in our experiments can hardly be explained by this model.

The QUILLS picture [24] yields a critical current density of 21.6 A m^{-1} for the Si devices investigated in this study. This exceeds the average critical current density obtained on our samples by about two orders of magnitude. The hot-electron picture

as proposed by Komiyama *et al* [16] applies for high Hall fields ($\epsilon_H > 40$ V cm^{-1}). It explains an S-shaped current–voltage characteristic and the rise of ρ_{xx} by several orders of magnitude as observed in the breakdown behaviour of the QHE on GaAs/GaAlAs heterojunctions. The rather smooth increase of ρ_{xx} at lower Hall fields (as present in our experiments) was described by an empirical relation of the form $\sigma_{xx} \sim \exp(\alpha\epsilon_H)$ and explained by thermal emission over an effective gap to delocalized states of the next higher Landau level.

Instead, we found an exponential dependence of ρ_{xx} in the QH regime on the reciprocal source–drain current with a slope depending on the filling factor (see figure 4). This corresponds to a Hall field dependence of the form $\rho_{xx} \sim \exp(\beta/\epsilon_H)$. This behaviour can be explained by a Zener tunnelling model [34] for intra-band transitions. Zener tunnelling as the relevant QHE breakdown mechanism was proposed by Tsui *et al* [20].

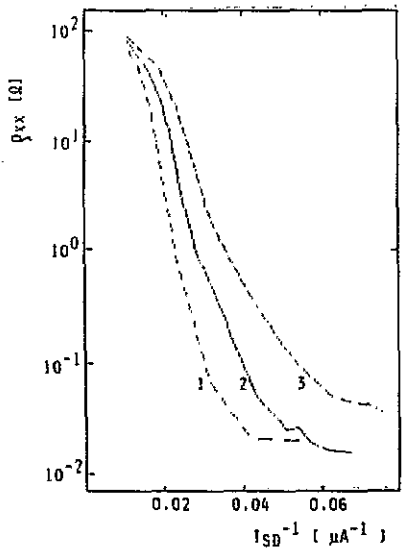

Figure 4. Resistivity ρ_{xx} at several gate voltages within the $i = 4$ plateau ($B = 11.56$ T, $T = 1.3$ K) of H IX versus the reciprocal source–drain current I_{SD}: 1, $V_g = 23.15$ V; 2, $V_g = 23.07$ V; 3, $V_g = 23.01$ V.

In this model, the rise of ρ_{xx} is due to the tunnelling of electrons from the Fermi energy to the next higher mobility edge of the quantum level along the Hall field and of holes in the opposite direction. This corresponds to a current component I_y parallel to the Hall field. Except for the Fermi energy being exactly in the middle between two levels (exactly integer filling factor), one of the tunnelling contributions (electrons for $\nu > i$, holes for $\nu < i$) is clearly dominating and both processes are equivalent for the same potential-well shape. This type of tunnelling is only adequate for real systems, because a momentum transfer, e.g. by phonons, is required to obey momentum conservation. Further, the ideal system is completely quantized even in the presence of a finite Hall field ϵ_H.

The presence of scatterers, however, resolves the degeneracy of the Landau eigenstates and leads to the formation of Landau bands and a non-zero DOS between them (e.g. [35]). This was explicitly shown on the samples investigated in this study [28]. Under these conditions, the tunnelling can be treated applying the Wenzel–Kramers–

Brillouin (WKB) tunnelling probability T for a saw-tooth potential [36]:

$$T = T_0 \exp\left[-4(2m^*)^{1/2} E_b^{3/2}/(3eh\epsilon_H)\right] \tag{3}$$

where T_0 = tunnelling prefactor(~ 1 [37]) and E_b = barrier height, i.e. difference between mobility edge and Fermi energy, with

$$V(y) = E_l - e\epsilon_H y \tag{4a}$$

where E_l = 2D bulk quantum level energy and

$$\epsilon_H = \rho_{xy} I_{SD}/w. \tag{4b}$$

The tunnelling current I_t of

$$I_t = \int_0^\infty T(E) f_1(E) D_1(E) [1 - f_2(E)] D_2(E)\, dE \tag{5}$$

where f_i = Fermi–Dirac function, $D_i(E)$ = density of states and $i = 1, 2$ = starting and final states, is proportional to the dissipative current component I_y responsible for the non-zero E_x component measured in the experiment. Equations (3) and (5) provide an explanation for the different slopes of the $\rho_{xx}(1/I_{SD})$ traces in figure 3. The larger the deviation of ν from integer values, the smaller is the average E_b and hence the slope in figure 3 (note that $I_t \sim I_y$ and $E_x \sim I_y$). The threshold condition for QHE breakdown was taken according to [36] at

$$\lg(I_t) = f(I_{SD}) = 0. \tag{6}$$

The strong dependence of the critical current on the filling factor ν is explained via the ν-dependent barrier E_b according to:

$$dE_b \simeq eB\, d\nu/h D(E_F) \tag{7}$$

where E_F is the Fermi energy. In the QH regime, $D(E_F)$ is mainly determined by the constant background DOS, which we evaluated by activation energy measurements (see [28]). Using these DOS and the Hall fields according to equation (4*b*), we obtained critical current dependences $I_c(\nu)$ as shown in figure 5 in comparison with the experimental ones. The agreement is quite satisfactory for the MOS sample (H VII), whereas the calculated results are markedly higher for the MNOS sample (H IX). It should be noted that neither the parameter T_0 (equation (3)) nor condition (6) were modified to adjust the calculations to the experimental results. We attribute the differences obtained for sample H IX to a reduced current path width leading to an enhanced Hall field (equation (4*b*)). Hence, we used the model to calculate the effective current path width w_{eff} as a function of the filling factor by adjusting the Hall field ϵ_H to the observed $I_c(\nu)$ dependences (taken at $\rho_{xx}^{th} = 1\ \Omega$). Figure 6 shows the result of these fits for sample H VII (MOS) and sample H IX (MNOS).

Both samples show a considerable decrease of the effective width $w_{eff}(\nu)$ with increasing deviation $\Delta\nu$ from the middle of the plateau at $\nu = i = 4$ ($i = 4$ has to be omitted because of the equal tunnelling rate for electrons and holes; see above). Furthermore, the dependence is steeper and at lower values for the MNOS sample

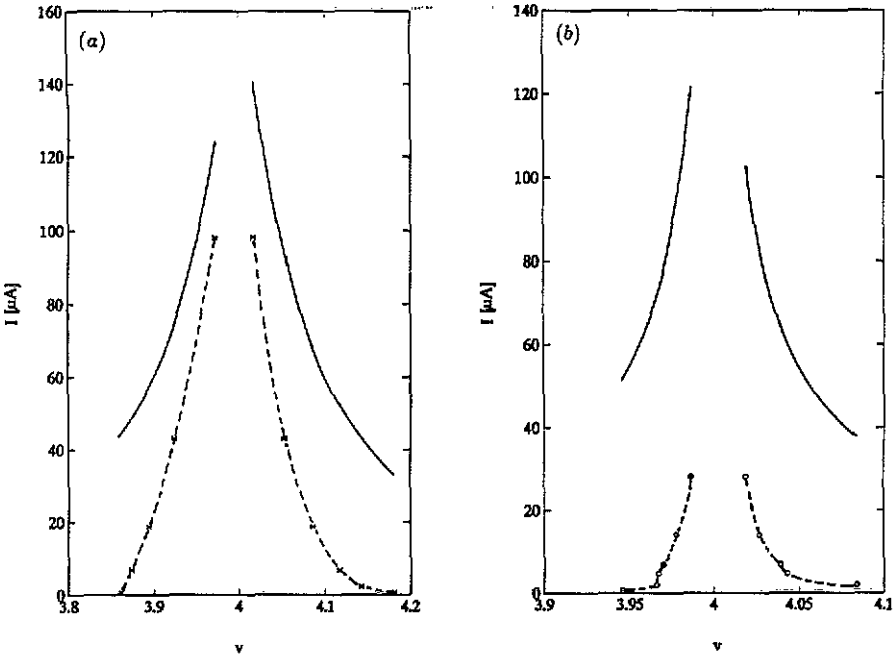

Figure 5. Filling-factor dependence of the critical current of the $i = 4$ plateau (full curves, tunnelling model (homogeneous Hall field over the entire sample width); broken curves, experimental data at $\rho_{xx}^{th} = 1\ \Omega$) for (*a*) sample H VII (×) and (*b*) sample H IX (○).

with the higher mobility and a DOS between the Landau levels of about half the value of the MOS sample [28]. That cannot be a simple consequence of the different DOS in equation (7), which accounts for a faster decrease of the critical current I_c with $\Delta\nu$ for the lower DOS at a given sample width w. A likely explanation is that the current path of the MNOS sample is narrower due to stronger inhomogeneities in it caused by long-range potential fluctuations (see above and [38]).

Of course, the fact of a reduced effective sample width due to potential fluctuations implies non-linear Hall fields and restricts the validity of our simple model to more qualitative aspects. However, the reduction of the current path width at the 'ends' of a plateau agrees well with the observations of the potential and current distribution in samples with internal contacts (see e.g. [30]) under QH conditions.

At low currents ($I_{SD} < 18\ \mu$A for sample H VII; see figure 3(*a*)), the plateau width decreases remarkably with increasing current. At higher currents, the sample shows slightly higher dissipation and at currents above $I_{SD} \simeq 40\ \mu$A we find another low dissipative regime with only a slight decreasing plateau width with the current. This behaviour was particularly pronounced at low values of ρ_{xx}^{th} or at low rates of dissipation apart from the current contacts. This is a strong indication for the existence of another breakdown mechanism at lower currents.

The validity of tunnelling considerations to explain the breakdown of the QHE is restricted to the current region with relatively high Hall fields ϵ_H. Here the 2D bulk carries the Hall current in a current path of variable width (see figure 6). At currents below the intermediate slightly higher dissipative state, the critical current changes less with the filling factor. In this low current range another current-carrying regime

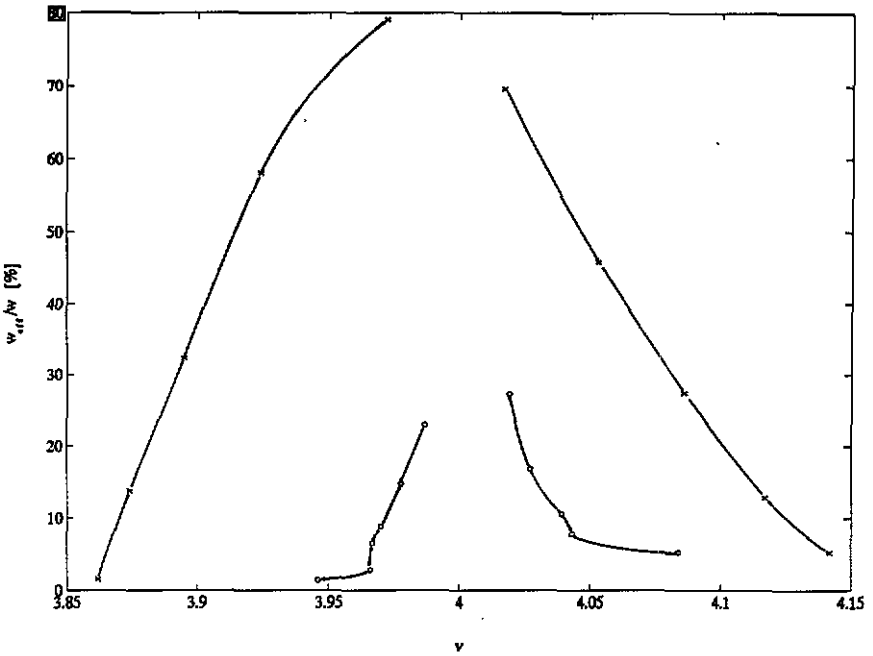

Figure 6. Effective current path width $w_{\rm eff}/w$ as a function of the filling factor ν (calculated from the experimental data of H VII (×) and H IX (○) applying the Zener tunnelling model—see text). The current path of the sample with a higher Hall mobility (H IX) is markedly narrower.

(edge states) might be dominating until a critical electrical field value above which the electrons are driven into bulk Landau-level states [6–8]. Our measurements in other current-injecting and voltage-probing configurations and on Corbino rings on the same chip confirm this assumption (see section 3.2).

3.2. Dependence of the breakdown of the quantum Hall effect on the current-injecting and voltage-probing contact configuration

The Corbino devices C VII and C IX located on the chips VII and IX were investigated under similar physical conditions as the Hall bars ($T = 1.3$ K, $B = 11.56$ T) in the range of the source–drain voltage 3.5 mV $\leqslant V_{\rm SD} \leqslant$ 20 mV. To make the data comparable to those obtained on the Hall bars, we used the condition $\sigma_{xx} \ll \sigma_{xy}$ in the plateau region, leading to the relation

$$\rho_{xx} \simeq \sigma_{xx}/\sigma_{xy}^2 = \sigma_{xx}(h/ie^2)^2 \tag{8}$$

to define the threshold condition $\rho_{xx} \leqslant \rho_{xx}^{\rm th}$.

The ring current I_y driven by the source–drain voltage $V_{\rm SD}$ in the Corbino ring under QH conditions ($\sigma_{xx} \to 0$, $I_x \to 0$) can be determined according to the following relation:

$$I_y = V_{\rm SD} ie^2/h. \tag{9}$$

Hence, it is possible to obtain the plateau width as a function of the channel current in comparison to the data obtained on the Hall bars. Figure 7 shows the corresponding

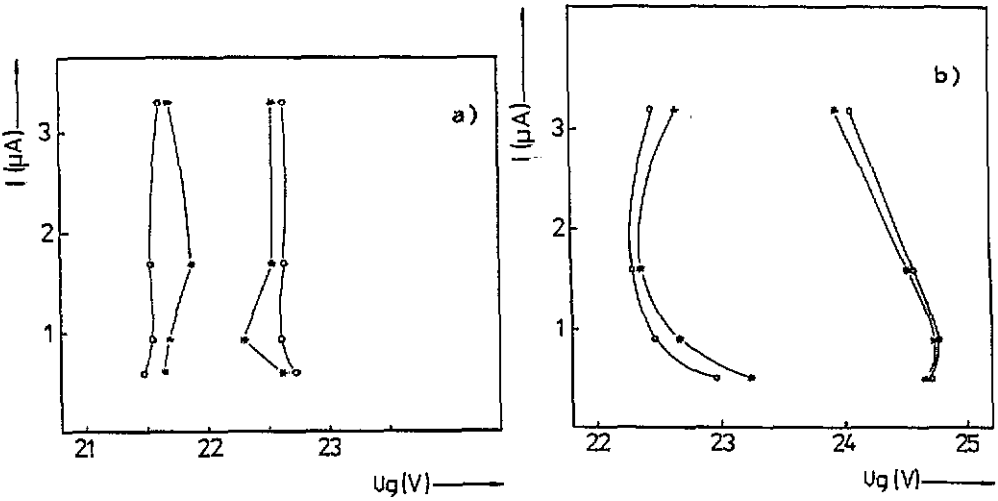

Figure 7. Gate voltage range of the $i = 4$ plateau ($B = 11.56$ T, $T = 1.3$ K) of the Corbino devices for (*a*) sample C VII (MOS) and (*b*) sample C IX (MNOS): (*) $\rho_{xx} < 0.1\ \Omega$; (O) $\rho_{xx} < 1\ \Omega$.

dependences for the Corbino samples C VII (MOS, figure 7(*a*)) and C IX (MNOS, figure 7(*b*)).

Both the Hall bars and the Corbino rings of the MOS samples show higher critical currents than the MNOS ones. The $i = 4$ plateau of the MOS Hall bar breaks down at $I_{SD} = 100\ \mu$A and of the MNOS Hall bar at $I_{SD} = 30\ \mu$A using $\rho_{xx}^{th} = 0.1\ \Omega$. This corresponds to average critical current densities of $j_c = 0.33$ A m^{-1} (MOS) and 0.10 A m^{-1} (MNOS). The same tendency was obtained on the Corbino rings on the same chips. The source–drain voltage range 3.5 mV $\leqslant V_{SD} \leqslant$ 20 mV corresponds to ring currents between 0.54 and 3.1 μA. The MNOS Corbino ring presents a noticeable reduction of the plateau width above $I_y = 2\ \mu$A. The strong increase of the plateau width below $I_y = 2\ \mu$A indicates a transition to bulk-dominated transport with increasing Hall field (see above). The edge current regime (strong reduction of the plateau width at low currents) could not be resolved for this sample at ring currents above the lowest accessible amount of 0.54 μA. An estimate of the maximum critical current density yields $j_c = 0.05$ A m^{-1}, which is about half the value of that of the adjacent Hall bar on the same chip. It is to be expected that the potential distribution inside a Corbino ring is different from that of a Hall bar, leading to a higher local current density near the inner electrode. This could give a qualitative explanation of the effect. However, this comparison only partially applies in view of section 3.1 because of the reduced current path width. This width is determined by the individual local potential shape of each sample.

The plateau width of the MOS Corbino sample shows a slight increase above $I_y = 2\ \mu$A. This current is obviously far below the critical value. Below 2 μA, both Corbino samples show an increase of the plateau width with current, but more pronounced and starting at lower ring currents for the MNOS sample. This is similar to our observations on most of the MOS Hall bars, and we attribute this to a switch from edge- to bulk-dominated current transport at a certain current (or Hall field) level.

To prove this, we investigated the filling-factor-dependent breakdown behaviour on

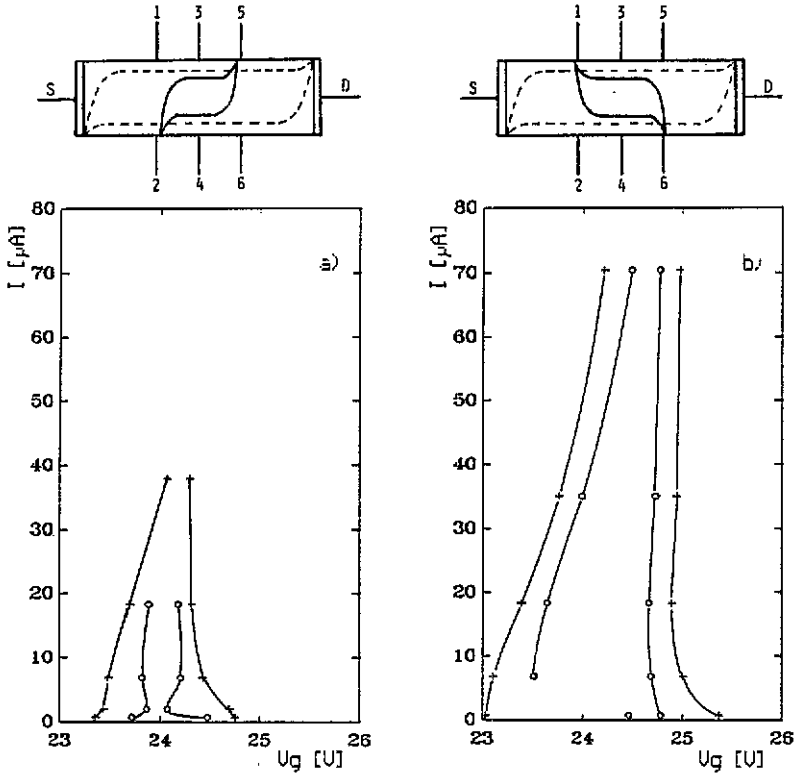

Figure 8. Gate voltage range of the $i = 4$ plateau ($B = 11.56$ T, $T = 1.3$ K) of the MOS sample H VI for the current fed into contacts (*a*) 2 and 5 (voltage at 4 and 6) and (*b*) 1 and 6 (voltage at 2 and 4): (○) $\rho_{xx} < 1\ \Omega$; (+) $\rho_{xx} < 10\ \Omega$. The sketches above (*a*) and (*b*) show the current-injecting and voltage-probing contacts and the equipotential lines (full curves) with respect to the 'normal' equipotential lines (broken curves)—see text.

Hall bars for different current-injecting and voltage-probing configurations. Figures 8(*a*) and (*b*) show the results of those measurements on the MOS sample H VI. The sketches above figures 8(*a*) and (*b*) depict the current and voltage contacts used with respect to the 'normal' equipotential line distribution. The data of figure 8(*a*) correspond to the current injected and drawn at the potential contacts 2 and 5 next to the potential jumps at the source and drain contacts in the 'normal' current-injecting configuration. This means that the current is injected parallel to the sample edge into the mean current flow direction. In this case, a rapid decrease of the plateau width with current up to 2 μA is observed. At higher currents the plateau widens again (the lower ρ_{xx}^{th} and hence the rate of dissipation apart from the current contacts, the more this effect is pronounced) and disappears at a current level of about 40 μA. This critical current is less than half the value obtained in the 'normal' configuration on the same sample (see section 3.1, figure 3(*b*)). Figure 8(*b*) shows the result obtained with the current being injected and drawn at the potential contacts 1 and 6 lying at the opposite diagonal with respect to the 'normal' potential jump corners at the source and drain contacts. In the sketch above figure 8(*b*) the actual potential jumps for this configuration are marked. From this it can be seen that the current is injected opposite to the main current flow direction. In this case, the behaviour of the QHE

breakdown is almost the same as in the 'normal' configuration. The low current decay of the plateau width is less pronounced and the maximal critical current amounts to 100 μA. This can be due to an immediate electron transfer from the injection point at the sample edge deeply into the 2D bulk because of the peculiar shape of the equipotential lines in this configuration.

We could not verify any significant influences of the current polarity and the choice of the voltage-probing potential contacts on the breakdown behaviour (see e.g. [37]) of our samples as long as the magnetic field polarity and the configuration of the current contacts remained unchanged. This is not surprising with regard to the long distances between the potential contacts (500 μm) and between source or drain and the next potential probe (1 mm). These distances certainly exceed the edge state equilibration length of the order of 100 μm [6].

From these findings on Si MIS devices we can make the following conclusions:

The low dissipative current flow mechanism of the QHE depends on the current level. At very low currents, the critical current is only weakly dependent on the filling factor and might be dominated by edge currents. At higher currents, in the vicinity of the plateau centre, a rather wide current path in the 2D bulk is established.

In agreement with [3], we conclude that the breakdown of the QHE is a local phenomenon. The width of the current-injecting contact is of less importance than its position with reference to the potential distribution (Hall field polarity). Current paths established within the 2D bulk are apparently capable of carrying much higher low dissipative currents than edge states.

4. Summary

We have investigated the breakdown of the low dissipative state of the QHE as a function of the filling factor on Si MOS and Si MNOS samples with the same geometry. The critical current at integer filling factors ($\nu = i = 4$) is about 100 μA for MOS and about 30 μA for MNOS Hall bars of 300 μm width. We attribute this to a smaller current path width in the MNOS sample caused by long-range potential fluctuations. This proposal is the result of the application of a simple tunnelling model, which is used to calculate the filling-factor dependence of the effective current path width by adjusting the effective Hall field to the experimentally determined critical currents.

At low currents, a remarkable reduction of the plateau width with increasing current occurs. This is attributed to another current-carrying mechanism (edge currents), which disappears above a critical Hall field.

We could confirm this assumption by measurements using several current-injecting and voltage-probing contact configurations on Hall bars. For currents injected parallel to the main current flow direction, the critical current is low and the two low dissipative regimes mentioned above are well separated in the breakdown behaviour. If the current is injected antiparallel to the main current flow direction, the critical current is as high as in the 'normal' configuration. In this case the current reaches bulk states at rather low Hall fields owing to the peculiar shape of the equipotential lines near the contacts.

Corbino rings located on the same chips showed qualitatively the same breakdown behaviour as the adjacent Hall bars, but at lower average current densities.

Acknowledgments

The authors are indebted to the Deutsche Forschungsgemeinschaft (DFG) for financial support. The samples were produced by the Institute of Semiconductor Physics, Frankfurt/Oder. We thank Dr L Smrčka for valuable discussions.

References

[1] Dorda G 1990 *Superlatt. Microstruct.* **7** 103
[2] Hajdu J and Janssen M 1990 *Phys. Bl.* **46** 426
[3] van Son P C, Kruithof G H and Klapwijk T M 1990 *Phys. Rev.* B **42** 11 267
[4] van Son P C, de Vries F W and Klapwijk T M 1991 *Phys. Rev.* B **43** 6764
[5] Syphers D A, Killoran J H, Brakewood H E, Reis F and Stiles P J 1990 *Surf. Sci.* **229** 37
[6] Alphenaar B, McEuen P L, Wheeler A G and Sacks R N 1990 *Phys. Rev. Lett.* **64** 677
[7] McEuen P L, Szafer A, Richter C A, Alphenaar B W, Jain J K, Stone A D and Wheeler R G 1990 *Phys. Rev. Lett.* **64** 2062
[8] Svoboda P, Středa P, Nachtwei G, Jaeger A, Cukr M and Láznicka M 1992 *Phys. Rev.* B at press
[9] Fontein P F, Hendriks P and Wolter J H 1990 *Surf. Sci.* **229** 47
[10] Fontein P F, Kleinen J A, Hendriks P, Blom F A P, Wolter J H, Lochs H G M, Driessen F A J M, Giling L J and Beenakker C W J 1991 *Phys. Rev.* B **43** 12 090
[11] Büttiker M 1988 *Phys. Rev.* B **38** 9375
[12] Ebert G, von Klitzing K, Ploog K and Weimann G 1983 *J. Phys. C: Solid State Phys.* **16** 5441
[13] Cage M E, Dzuiba R F, Field B F, Williams E R, Girvin S M, Gossard A C, Tsui D C and Wagner R J 1983 *Phys. Rev. Lett.* **51** 1374
[14] Kuchar F, Bauer G, Weimann G and Burkhard H 1984 *Surf. Sci.* **142** 196
[15] van Son P C, Kruithof G H and Klapwijk T M 1990 *Surf. Sci.* **229** 57
[16] Komiyama S, Takamasu T, Hiyamizu S and Sasa S 1985 *Solid State Commun.* **54** 479
[17] Středa P and von Klitzing K 1984 *J. Phys. C: Solid State Phys.* **17** L483
[18] Trugman S A 1983 *Phys. Rev.* B **27** 7539
[19] Pokrovsky V L, Pryadko L P and Talapov A L 1990 *J. Phys.: Condens. Matter* **2** 1583
[20] Tsui D C, Dolan G J and Gossard A C 1983 *Bull. Am. Phys. Soc.* **28** 365
[21] Kirtley J R, Schlesinger Z, Theis T N, Millikan F P, Wright S L and Palmateer L F 1986 *Phys. Rev.* B **34** 1384
[22] Bliek L, Hein G, Niemeyer J, Weimann G and Schlapp W 1987 *Springer Ser. Solid-State Sci.* **71** 113
[23] de Vegvar P G N, Chang A M, Timp G, Mankiewich P M, Cunningham J E, Behringer R and Howard R E 1987 *Phys. Rev.* B **36** 9366
[24] Eaves L and Sheard F J 1986 *Semicond. Sci. Technol.* **1** 346
[25] Kirtley J R, Schlesinger Z, Theis T N, Millikan F P, Wright S L and Palmateer L F 1986 *Phys. Rev.* B **34** 5414
[26] Cage M E, Marullo Reedtz G, Yu D Y and Vandergrift C T 1990 *Semicond. Sci. Technol.* **5** 351
[27] Nachtwei G, Breitlow C, Salchow O, Krüger H and Herrmann R 1990 *Semicond. Sci. Technol.* **5** 1088
[28] Nachtwei G, Salchow O, Breitlow C, Jaeger A and Krüger H 1991 *Surf. Sci.* **250** 243
[29] Weast R C, Astle M J and Beyer W H 1983-84 *Handbook of Chemistry and Physics* 64th edn (Boca Raton, FL: CRC Press)
[30] Ebert G, von Klitzing K and Weimann G 1985 *J. Phys. C: Solid State Phys.* **18** L257
[31] Zheng H Z, Tsui D C and Chang A M 1985 *Phys. Rev.* B **32** 5506
[32] Woltjer R, Eppenga R and Schuurmanns M F H 1987 *Springer Ser. Solid-State Phys.* **71** 104
[33] McDonald A H, Rice T M and Brinkman W F 1983 *Phys. Rev.* B **28** 3648
[34] Zener C 1934 *Proc. R. Soc. Lond.* **145** 523
[35] Gerhardts R R and Gudmundsson V 1986 *Phys. Rev.* B **34** 2999
[36] Sze S M 1981 *Physics of Semiconductor Devices* (New York: Wiley)
[37] Blochinzew D I 1953 *Grundlagen der Quantenmechanik* (Berlin: Deutscher Verlag der Wissenschaften)
[38] Sachrajda A S, Landheer D, Boulet R and Moore T 1989 *Phys. Rev.* B **39** 10 460